



Effect of Structural Change on Temperature Behavior of a Long-Span Suspension Bridge Pylon

Jungwhee Lee¹ · Kenneth J. Loh² · Hyun Sung Choi¹ · Hohyun An¹

Received: 4 January 2019 / Accepted: 13 September 2019 / Published online: 18 September 2019
© Korean Society of Steel Construction 2019

Abstract

The effect of structural changes on the temperature behavior of a long-span bridge pylon was examined using field-measured data and finite element (FE) analysis. Temperature behavior of the pylon could be modeled using two characteristic parameters, α and β , which reflect the influence of the variation in the ambient temperature and the sectional temperature difference, respectively. Two major structural changes namely, decrease in stiffness in the lower region of the pylon and decrease in area of the main cable were considered in the FE analyses, which showed that both α and β were affected by the structural changes. Furthermore, the two characteristic parameters could be extracted with sufficient accuracy from field-measured temperatures and tilting angle data using a system-identification technique. Consequently, the feasibility of identification of structural changes by continuous observation of temperature parameters was demonstrated. However, the tilting angle of the pylon is influenced by other loads than the temperature and therefore future studies on eliminating other loading effects (such as that owing to wind or traffic) are necessary.

Keywords Long-span suspension bridge · Pylon · Tilting angle · Structural change · Temperature behavior · FE analysis

1 Introduction

Bridge structures experience member-temperature variation due to daily and yearly variation of the ambient temperature. The static and dynamic behaviors of a bridge are affected by these temperature variations, especially in places that experience distinct seasons.

Many long-span bridges built in the recent few decades are equipped with structural health monitoring systems,

which include sensors for evaluating structural behaviors (such as the displacement, tilting angle, acceleration, and strain) as well as sensors for determining the loading effect such as that owing to the wind speed/direction, earthquakes, weights of vehicles, and temperatures (Wong 2004; Kim et al. 2005; Koh et al. 2005; Chang et al. 2009; Ou and Li 2010).

Several previous investigations of the temperature behavior of bridges have focused on the temperature load, which is correlated with the sectional temperature distribution, thermal stress/strain, and thermal flexure. These studies concentrated on developing design methods that consider the thermal effects, and recent investigations have focused on code improvement using field-measured sectional temperature distributions (Roberts-Wollman et al. 2002; Fu and DeWolf 2004).

Studies on the variation of the sensitivity of the sensors and the changes in the structural behavior due to temperature variations have been performed in the field of health monitoring system design and structural damage detection. In these studies, the effect of the temperature variations was considered detrimental, which therefore must be compensated for or eliminated (Sohn et al. 1999; Park et al. 1999, 2003; Lynch and Loh 2006; Magalhaes et al. 2012).

✉ Hyun Sung Choi
hschoi112@dankook.ac.kr

Jungwhee Lee
jwhee2@dankook.ac.kr

Kenneth J. Loh
kenloh@ucsd.edu

Hohyun An
truelies9601@gmail.com

¹ Department of Civil and Environmental Engineering, Dankook University, 152 Jukjeon-ro, Yongin-si 16890, Republic of Korea

² Department of Structural Engineering, University of California-San Diego, 9500 Gilman Drive, La Jolla, CA 92093, USA

The temperature behavior of cable-stayed bridges (Cao et al. 2010), suspension bridges (Kim et al. 2005; Xia et al. 2013; Chang et al. 2008; Xu et al. 2010; Koo et al. 2013), and a long-span tied arch bridge (Yarnold and Moon 2015) has been evaluated. These studies focused mainly on the effect of temperature variation on the static and dynamic behavior of the bridges. Chang et al. assessed the temperature behavior of the Yeongjong Bridge, a self-anchored suspension bridge. They reported that the bridge response may be predicted by an ARX model, and the health status of the bridge can be assessed by analyzing the residuals between the predicted and measured responses (Chang et al. 2008). Moreover, Xia et al. (2013) examined the temperature behavior of the Tsing Ma Suspension Bridge, and proposed that the temperature-behavior pattern can be used as a damage indicator. Furthermore, studies on the temperature behavior of large-span roof structures, a type of long-span structure, were also conducted (Liu et al. 2013; Zhao et al. 2017a, b). Similar to cases involving bridges, changes in the temperature affected the attributes such as deformations and reaction forces of long-span roof structures. However, the presence of the roof covering also affected the temperature distribution over the structure.

Therefore, the feasibility of assessing structural changes via temperature-behavior analysis is considered in this study. The Gwangsan Bridge, a suspension bridge located in Busan, South Korea, is selected for investigation, and the relationship between the tilting angle of the pylon and the temperature is examined using field-measured data. In addition, a finite element (FE) model of the bridge is used to calculate characteristic parameters of intact and modified structures.

2 Analysis of Field-Measured Data

2.1 Gwangsan Bridge

The Gwangsan Bridge (Busan, South Korea), a typical three-span simply supported suspension bridge that was opened to traffic in 2003 was considered in this study. The main span

length and total length of the bridge are 500 m and 900 m, respectively, as shown in Fig. 1a. The main components of the bridge (main cable, pylon, stiffening truss, and deck) are composed of structural steel. The stiffening truss supports a double deck (see Fig. 1b).

As shown in Fig. 2, the Gwangsan Bridge is built in the NE–SW direction, with an approximately 35° angle to the N–S direction. Therefore, compared with other surfaces, the south-facing surfaces of the bridge absorb more solar energy in the daytime.

The major sensors installed in the first pylon (PY1) are shown in Fig. 3. Ten thermocouples that measure the member temperature, a temperature sensor for the air temperature, and four tilt-meters were installed. Many other types of sensors were installed in the pylons and other parts of the bridge. However, only the sensors directly related to the current study are shown. Thermocouples for measuring the member temperature and tilt-meters were installed inside the pylon section and the air temperature was measured outside the pylon with a radiation shield. Technical specifications and photographs of the sensors are shown in Table 1.

2.2 Temperature Response of the Gwangsan Bridge

Variation of the temperature measured for PY1 during an 11-month period from November 1st to September 30th, 2017, are shown in Fig. 4. The measurement interval was 10 min. The first plot shows the air temperatures measured at the top of PY1 (THO1), and the second shows the average temperatures acquired from all 10 thermocouples (THP1–THP10) installed on PY1. The plots show that the air and member temperature varied from 0 °C to +35 °C; further, they show very similar patterns in the variation. Generally, temperatures of the steel structures that directly receive solar radiation are higher than the ambient temperatures, and maximum temperatures may exceed 60 °C (Liu et al. 2013; Zhao et al. 2017a, b). However, in this study, all 10 thermocouples (THP1–THP10) were installed inside the PY1. Considering the thickness of the steel plate of PY1 (40 mm) and the shelter effect, it is normal that the measured

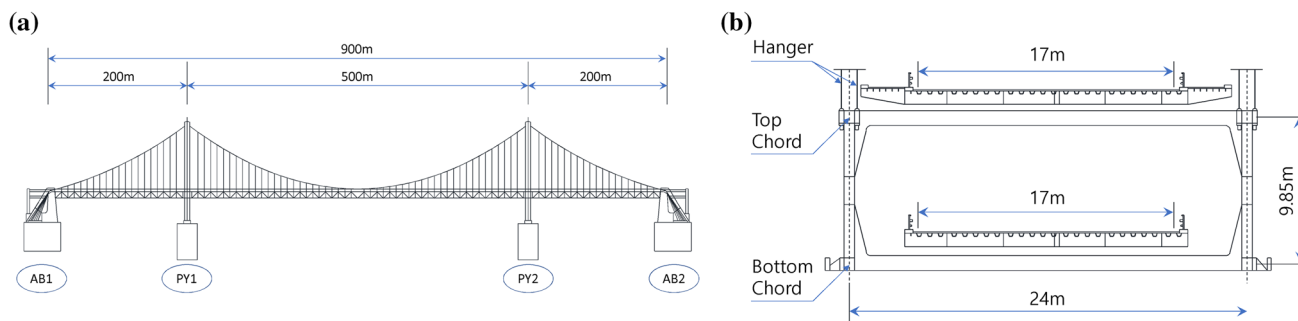


Fig. 1 Gwangsan Bridge overview. a Span length. b Cross-section of the stiffening truss



Fig. 2 Photograph of the Gwangang Bridge (Google Maps)

member temperatures were similar to or lower than the ambient temperature.

The temperatures measured by the two thermocouples installed on the NW-facing surface (THP9) and SE-facing surface (THP10) are shown in Fig. 5a, in which the ambient temperature variation is plotted. The difference between the two temperature signals is shown in Fig. 5b. Both thermocouples were located in the same section D–D. As Fig. 5a shows, the peak temperature of the SE-facing surface was higher than that of the NW-facing surface. These peak temperatures occurred at approximately noon and 6 pm (i.e., 6 h later) for THP10 and THP 9, respectively. As shown in Fig. 5b, the sectional temperature difference varied from $-2\text{ }^{\circ}\text{C}$ to $+8\text{ }^{\circ}\text{C}$, and the highest difference occurred at noon.

The tilting angle measured at the top of PY1 (Tilt3) is shown in Fig. 6. The data obtained during the entire 11-month period and in only 1 week are shown in Fig. 6a, b, respectively. Similar to the temperature data, clear yearly and daily

periodicity were observed. In comparison with the temperature data shown in Fig. 5a, the tilting angle curve shown in Fig. 6b includes a relatively much higher frequency component. It has been reported previously that this high-frequency response is caused by wind and traffic loads.

Figure 7 shows the dependence of the tilting angle on the ambient temperature for an 11-month period. The angle–temperature correlation was determined via linear regression, and a high coefficient of determination, R^2 , was obtained (>0.9). However, the simple linear regression performed here ignores the influence of the sectional temperature distribution. Therefore, additional consideration of the sectional temperature difference is required for a more accurate analysis.

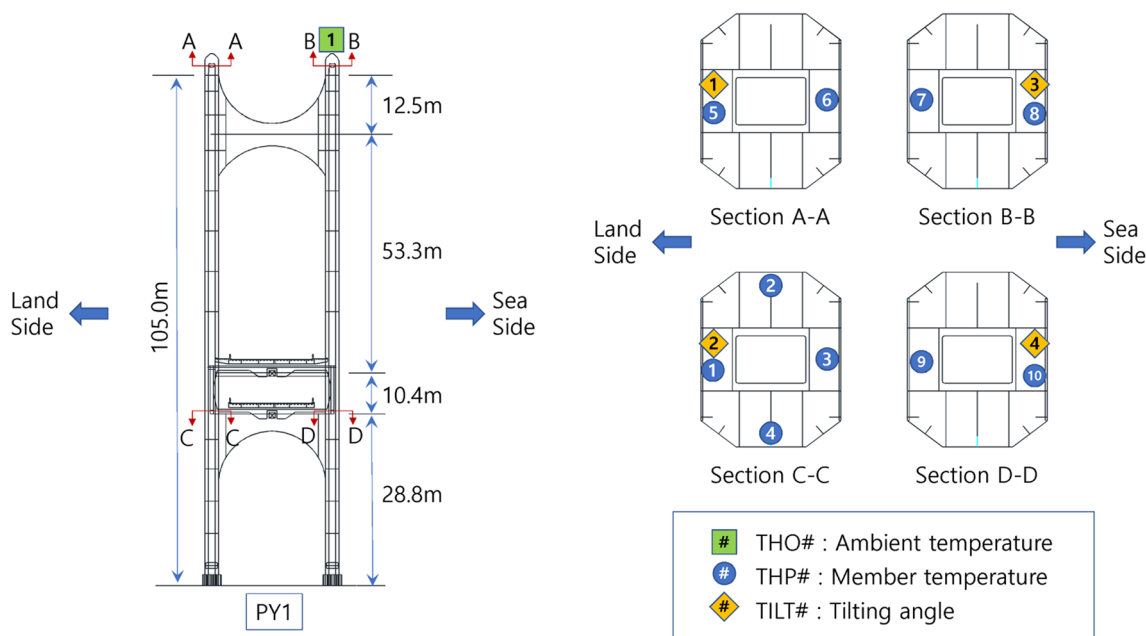

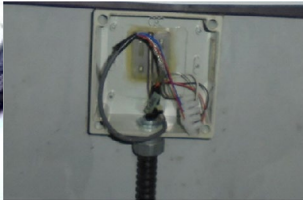



Fig. 3 Deposition of major sensors on PY1

Table 1 Specifications and photographs of the utilized sensors

Sensor	Tiltmeter	Thermocouple (member temperature)	Thermometer (air temperature)
Technical specification	Sensor type: electrolytic range: $\pm 8^\circ$ Resolution: $1 \mu\text{rad}$	Sensor type: RTD Range: -100 to $+200^\circ\text{C}$ Accuracy: $\pm 0.5^\circ\text{C}$	Sensor type: RTD Range: -30 to $+50^\circ\text{C}$ Accuracy: $\pm 0.3^\circ\text{C}$ at 0°C
Photograph			

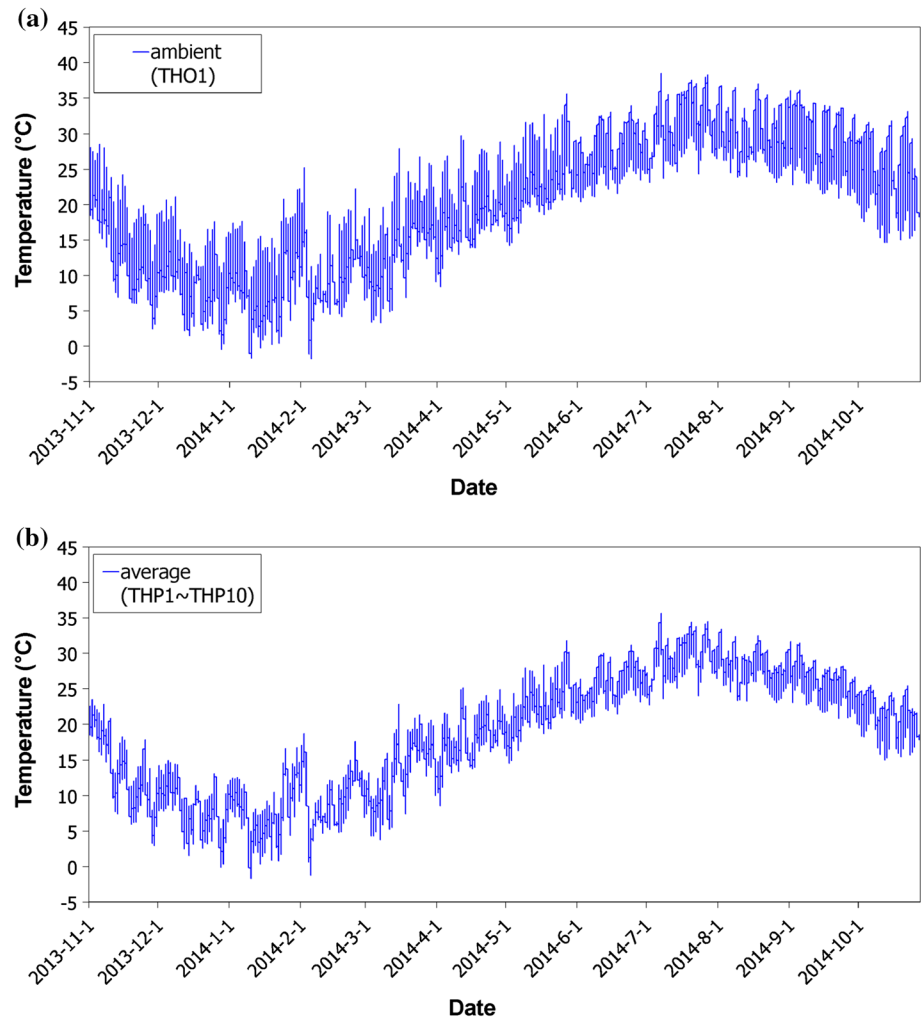
3 Validation of FE Model

3.1 FE model of the Gwangan Bridge

An FE model constructed within the scope outlined by a previous study (Kim et al. 2012) was employed for (1) numerical examination of the bridge response induced by a temperature load, and (2) determining the influence of structural changes on the temperature behavior. Model validation employing natural frequencies has been performed within the scope defined by a previous study. The overall shape of the three-dimensional (3D) FE model is shown in Fig. 8. The commercial general-purpose FE analysis software MIDAS-Civil was used (MIDAS IT 1996).

Truss elements were used to model the main cables and hangers, and initial tension was introduced using a pre-stressing command. The pylons and girders were modeled with beam elements and steel decks were modeled using shell elements. Fixed boundary conditions were applied to the lower ends of pylons and abutments. The section and material properties applied to the FE model were as shown in Table 2. A linear elastic material model was adopted, and no material nonlinearity was considered. Since the objective is the structure of a completed suspension bridge, not a suspension bridge under construction, the nonlinear behavior was not significant and the linear material model was sufficient for the purpose of this study.

Fig. 4 Yearly variation of temperatures. **a** Air temperature. **b** Pylon average temperature



3.2 FE Model Validation Using the Temperature Response

In a previous study, natural frequencies were employed for the model validation and, hence, additional validation using the temperature response was performed in the present study.

3.2.1 Influence of Ambient-Temperature Variation (α)

In the first case, a uniform temperature variation was applied to the FE model for the entire bridge structure. The resulting displacement was compared with the measured displacement to validate the structural behavior resulting from annual ambient-temperature variation. Considering the span of this variation, eight cases were evaluated where the temperature was varied from 0 to 35 °C in step sizes of 5 °C. The FE analysis results and the measured response are compared in Fig. 9. The initial value and sign were modified based on the measured data, and the calculated and measured responses exhibited a close correlation. A linear relation with a slope of 38.0 $\mu\text{rad}/^\circ\text{C}$ was determined from the FE analysis results,

and this denotes the first characteristic parameter for the pylon temperature behavior, α .

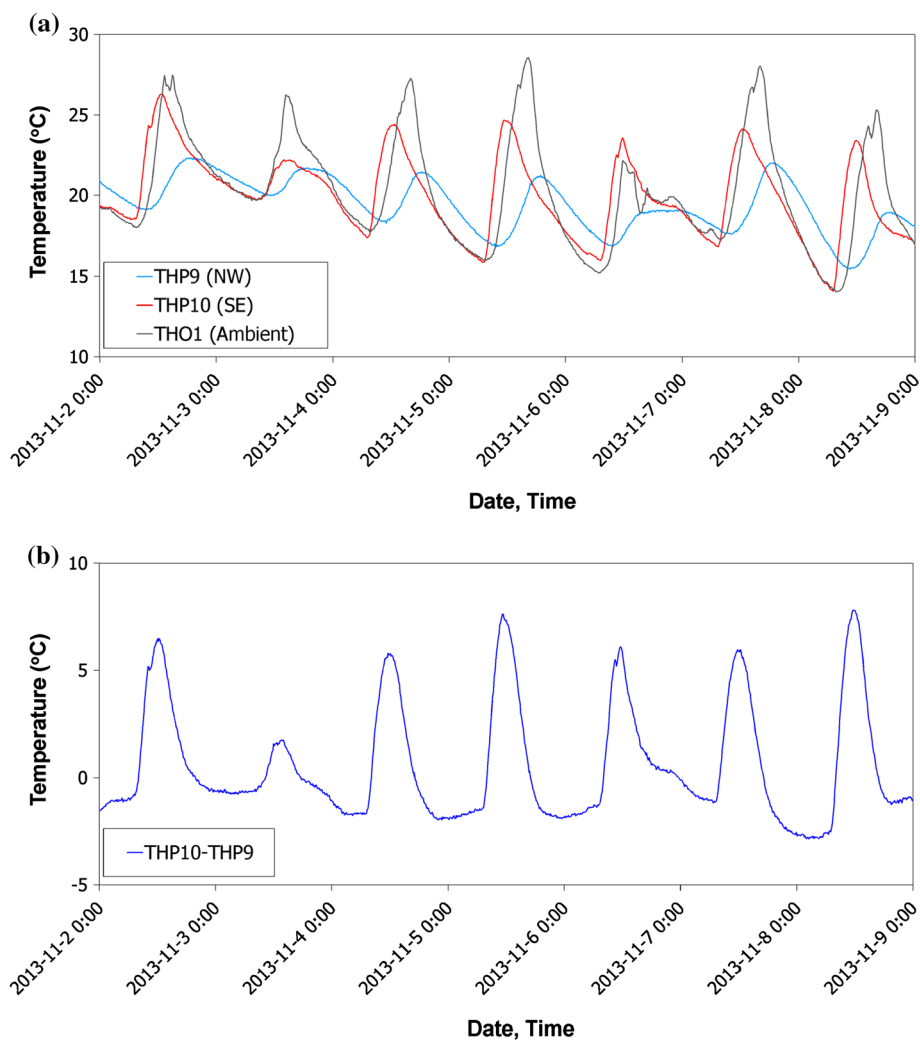
Deformed shapes corresponding to the two extreme cases (0 °C and 35 °C) are shown in Fig. 10. As the figure shows, the top of the pylon and midspan of the girder underwent outward displacement and upward displacement, respectively, during the winter.

3.2.2 Influence of the Sectional Temperature Difference (β)

As shown in Fig. 5b, a sectional temperature difference of approximately 10 °C occurred periodically between the SE- and NW-facing surfaces of Gwangang Bridge PY1, leading to additional flexure of the pylon. This additional flexural displacement was calculated by applying an equivalent uniform distributed load (UDL) to the pylon of the Gwangang Bridge 3D FE model.

To determine the UDL equivalent to the temperature load, one leg of the pylon was modeled using shell elements, first. A temperature load of +10 °C was applied to the two surfaces facing the SE and SW directions, and the resulting

Fig. 5 Temperature variation in pylon section. **a** SE- and NW-facing surfaces. **b** Sectional difference



displacement on top of the leg was then determined. Then, the same leg of the pylon was subsequently modeled with beam elements, and unit UDLs in x and y directions were applied. Afterward, the magnitude of the UDLs was determined by comparing the two resulting sets of displacements calculated via the shell model and the beam model. The acquired UDL equivalent to +10 °C of the sectional temperature difference was 4.379 kN/m and 3.966 kN/m for in the x direction (axial direction) and y direction (lateral direction), respectively.

The equivalent UDL determined from the preceding procedures was applied to the global bridge model as shown in Fig. 11a, and the resulting deformation shape is shown in Fig. 11b. The tilting angle of the pylon top and the sectional temperature difference for this case were 98 μ rad and +10 °C, respectively. These values yielded a value of 9.8 μ rad/°C for the sensitivity of the tilting angle to the sectional temperature difference, and this constitutes the second characteristic parameter for the pylon temperature behavior, β .

3.2.3 Re-generation of Tilting Angle Using Temperature Measurements and Characteristic Parameters

The two characteristic parameters, α and β , which represent the sensitivity of the tilting angle to variation in the ambient temperature and sectional temperature differences, respectively, were determined utilizing the aforementioned procedures. Values of 38.0 μ rad/°C and 9.80 μ rad/°C were obtained for these respective parameters. If the tilting angle calculated using these two parameters and the measured temperatures yield similar values to those of the measured tilting angles, the parameters obtained by FE analysis are considered representative of the bridge-temperature behavior. The utilized FE model is therefore adequate for the purpose of the present study.

In other words, if the FE model and both parameters α and β are adequate, the tilting angles calculated using Eq. (1) should be similar to the measured values. Therefore, the calculated response and the measured response were compared,

Fig. 6 Tilting angle variation (Tilt3). **a** Yearly variation. **b** Weekly variation

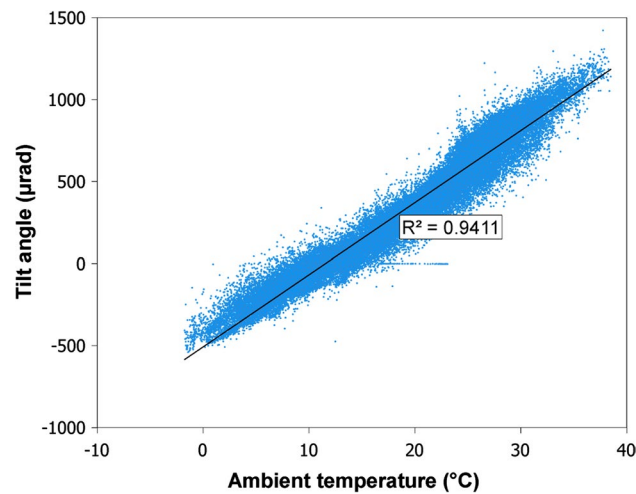
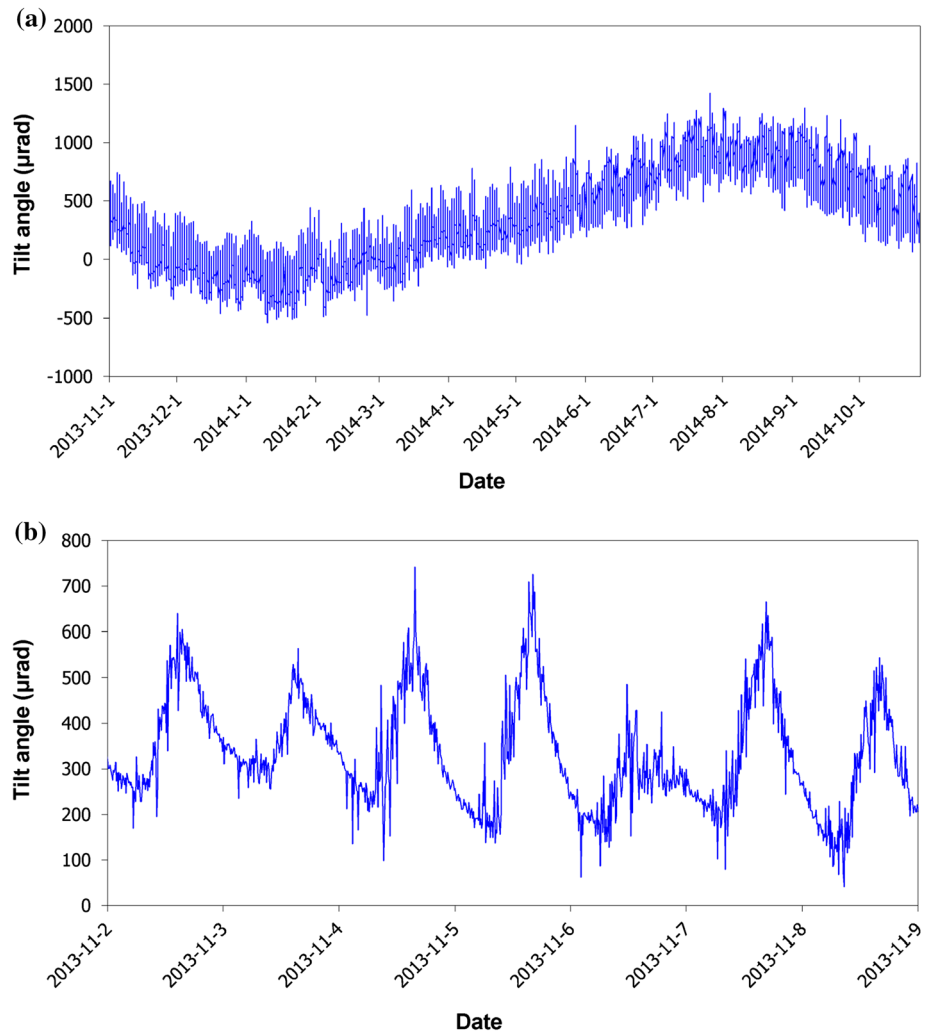


Fig. 7 Dependence of tilting angle on ambient temperature

and an appropriate constant C was added for initial-value correction.

$$(THO1) \times \alpha + (THP10 - THP9) \times \beta + C = \text{Tilt3} \quad (1)$$

where THO1, THP9, THP10, and Tilt3 are the names of the sensors (see Fig. 3 for the types and locations of these sensors).

A comparison of the calculated tilting angles and the measured responses (see Fig. 12) revealed that their values were quite similar.

Figure 13 shows the residual errors determined for the tilting angles measured and calculated in 1 month (i.e., December 2013). The data from all 11 months were analyzed in the same procedure. The residual analysis was performed for each month, and the average value, standard deviation, and square root of the sum of squares (SRSS) associated with the residual error were used for model confirmation. The analysis results are listed in Table 3. To eliminate the high-frequency response component, a moving average with six samples (1 h) was applied. As shown in Fig. 13 and

Fig. 8 Three-dimensional (3D) FE model of the Gwangan Bridge

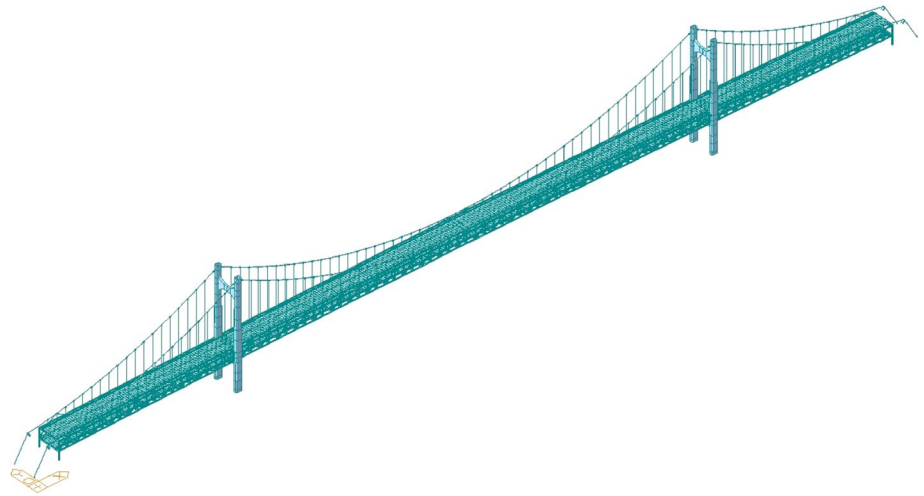


Table 2 Section and material properties

Member	E (kN/m ²)	A (m ²)	I (m ⁴)
Main cable	1.99E+08	0.2267	–
Hanger	1.37E+08	0.0079	–
Upper and lower chord member	2.06E+08	0.0672–0.0784	0.00521–0.00603
Vertical and diagonal member	2.06E+08	0.0371–0.106	0.0028–0.00959
Pylon	2.06E+08	0.7917–0.9415	2.667–5.102

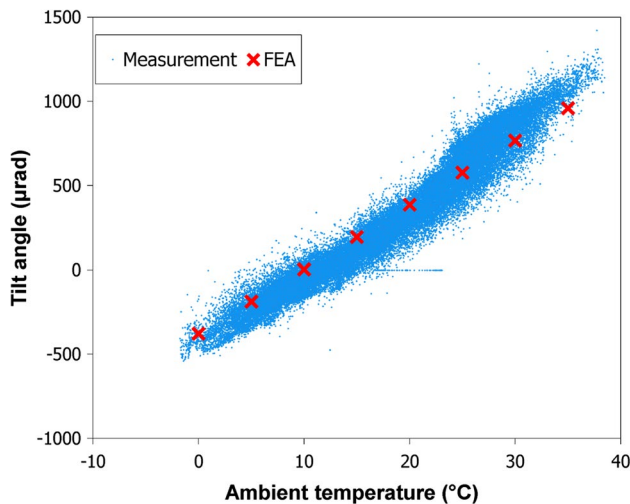


Fig. 9 Dependence of tilting angle on ambient temperature

Table 3, the residuals are described by a normal distribution (average: zero), and the standard deviation corresponding to each month was ≤ 70 μrad .

The results presented so far confirm the adequacy of the utilized FE model and reveal that the temperature response of the pylon tilting angle can be simplified by considering the two characteristic parameters α and β . Therefore, the influence of structural changes on these characteristic

parameters was examined via FE analysis in the subsequent phase of the study.

4 Influence of Structural Change on Characteristic Parameters

4.1 Scenario of Structural Change

Two types of structural change that severely affect the global behavior of suspension bridges were examined from the viewpoint of their influence on the characteristic parameters, α and β . These changes were decrease in the stiffness of the lower part of the pylon (Fig. 14a), and the decrease in the sectional area of the main cable (Fig. 14b). For clear examination of the influence, a broad range of changes was considered in each case.

4.1.1 Stiffness Decrease for Lower Part of Pylon

As shown in Fig. 3b, the pylon of the Gwangan bridge consists of a steel box section (wall thickness: 50 mm). For this structural change, the wall thickness of the lower 25 m of the pylon was reduced to 45 mm and 40 mm, and both temperature parameters were calculated for each case. The sectional coefficients corresponding to a height of 25 m from the base are listed in Table 4.

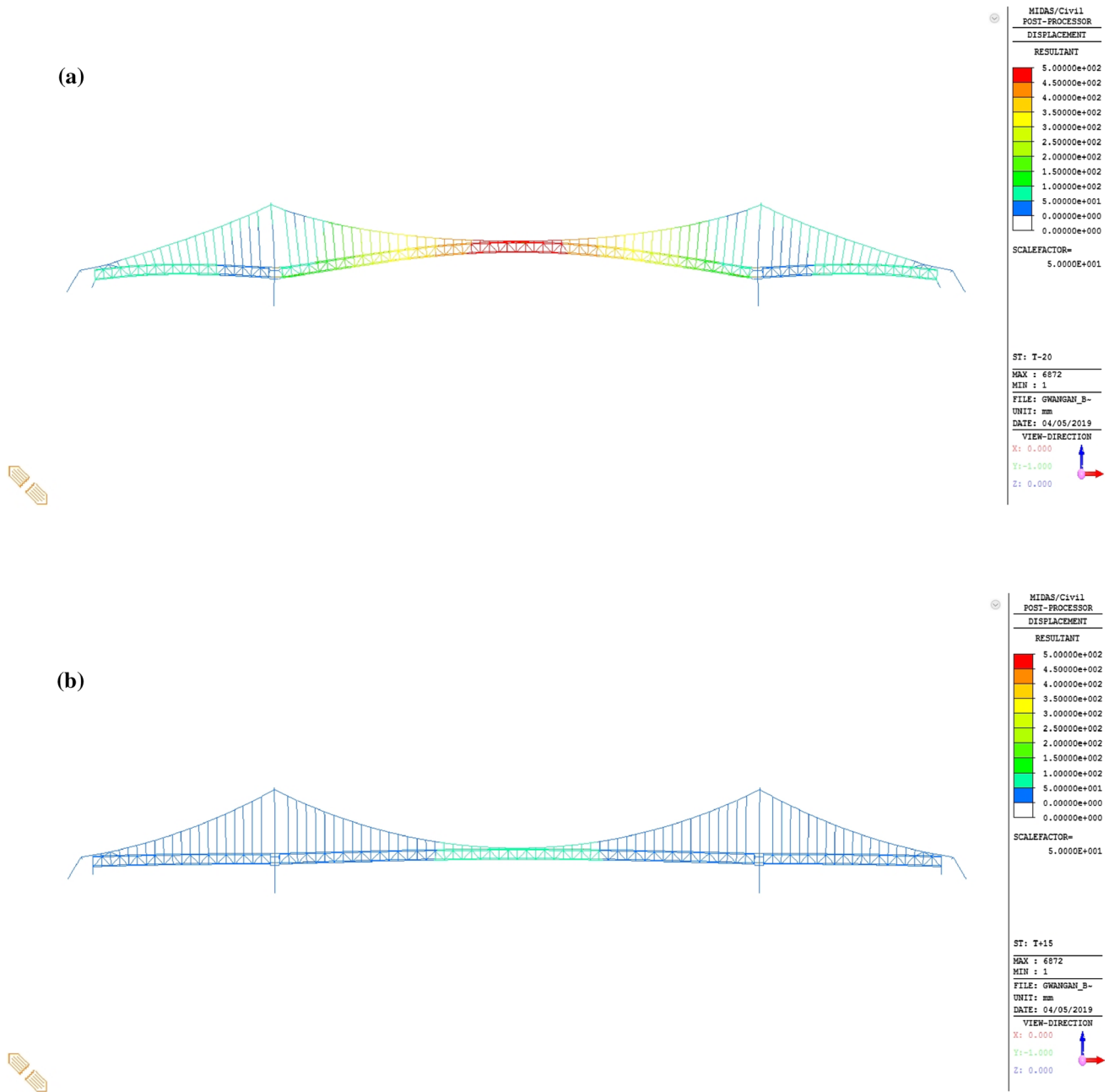


Fig. 10 Deformed shape induced by seasonal changes. a Winter (0 °C). b Summer (35 °C)

4.1.2 Sectional Area Decrease for Main Cable

In the FE model, the main cable was modeled as a circular solid section (sectional area: $2.267 \times 10^5 \text{ mm}^2$). For this structural change, the sectional area decreased to 90% and 80% of the initial area for cases DL C1 and DL C2, respectively, and both temperature parameters were calculated for each case (see Table 5 for the corresponding main-cable section areas).

4.2 Influence of Structural Change

4.2.1 Decrease in Stiffness of Lower Part of Pylon

The temperature parameters, α and β , both increased due to decrease in the stiffness of the lower part of the pylon. Changes in the ambient temperature resulted in thermal deformation of the main suspension cable, and an unbalanced force was generated in the longitudinal direction. As

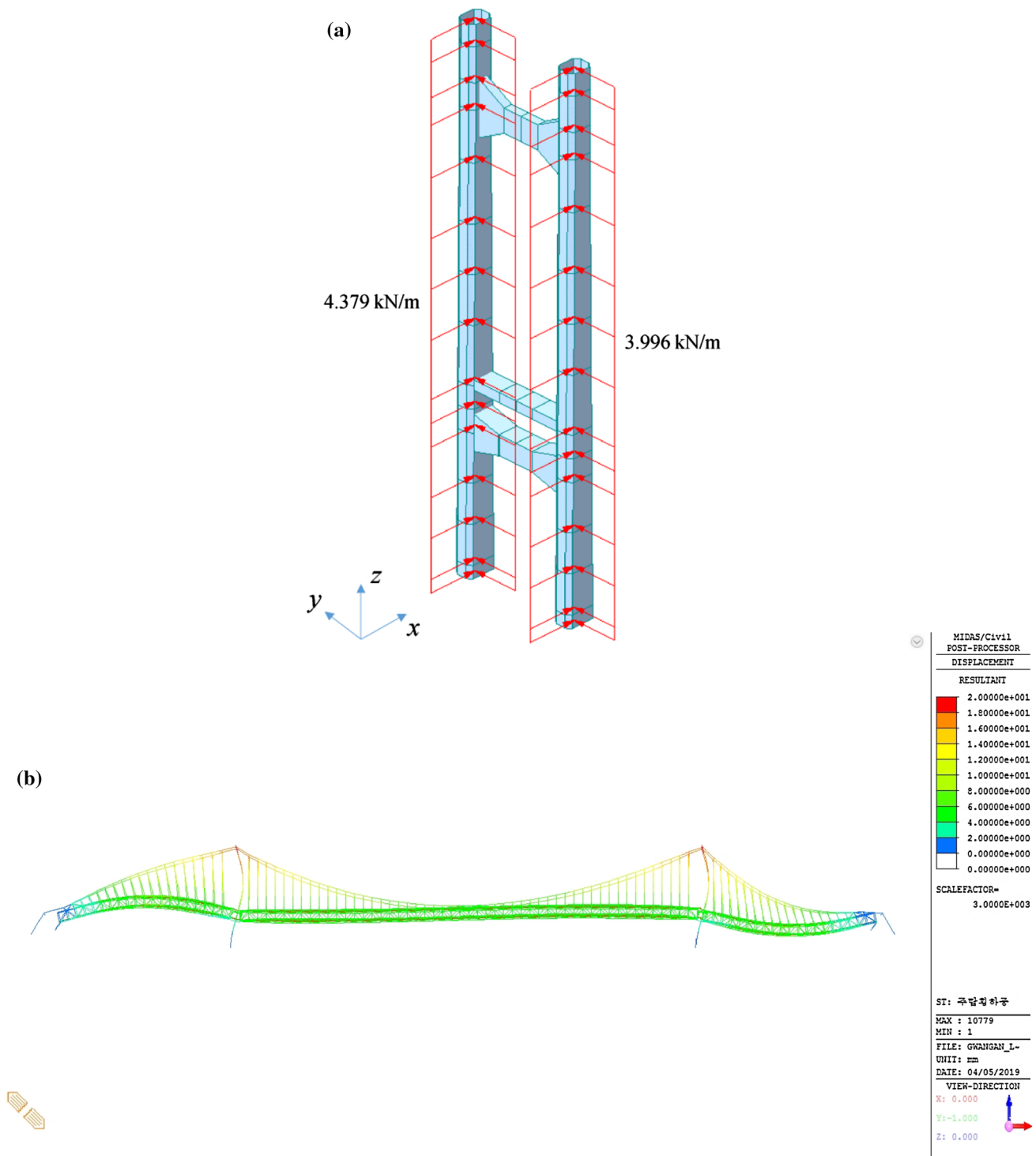


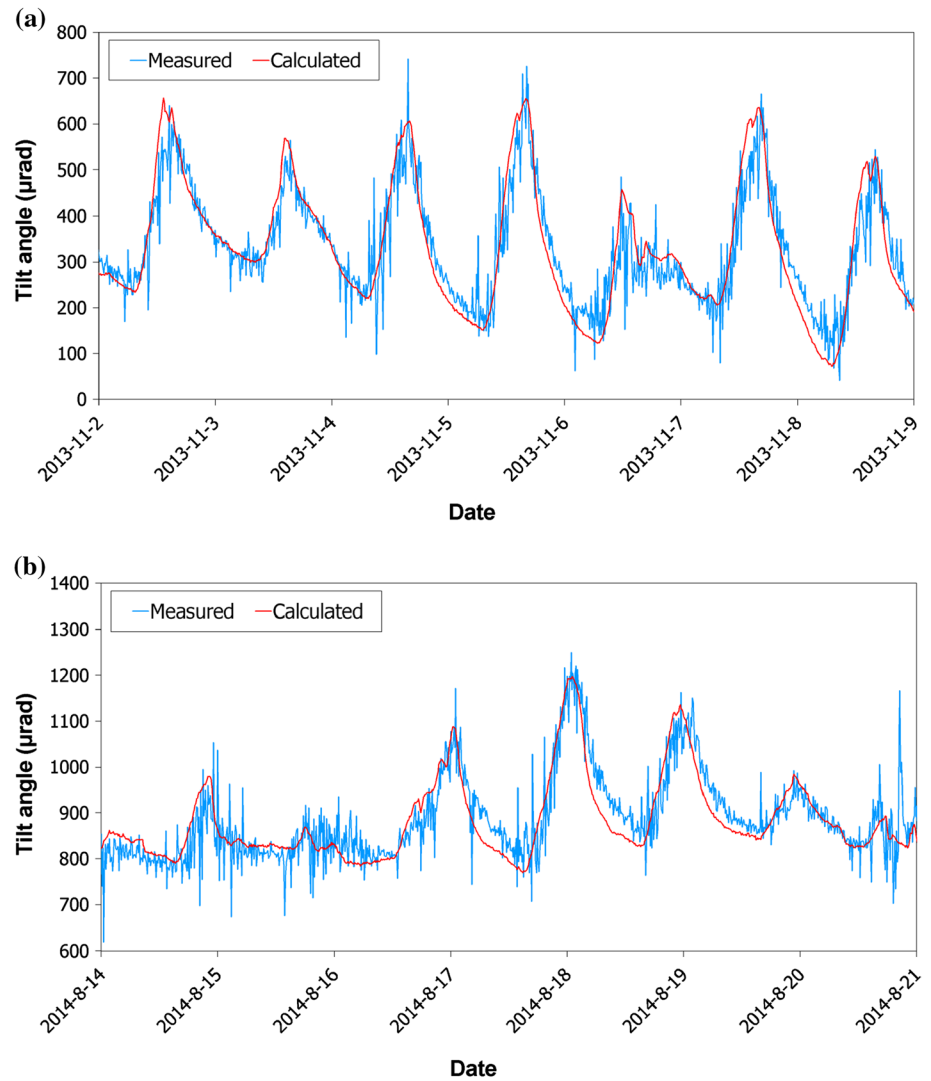
Fig. 11 Calculation of deformation due to sectional temperature distribution. **a** Equivalent uniform distributed load. **b** Deformed shape

a result, the pylon was deformed in one direction. If the stiffness of the pylon decreased, the deformation resulting from the same unbalanced force increased and, consequently, the sensitivity to ambient temperature, α , increased. Also, as a result of the decreased pylon stiffness, increased deformation

occurred for the same sectional temperature difference, and therefore the sensitivity to the sectional temperature difference, β , increased.

The changes in both temperature parameters and the 1st natural frequencies, as determined via FE analyses, are

Fig. 12 Comparison of tilting angle. **a** Winter (November 2013). **b** Summer (August 2013)



shown in Table 6. Structural change 1 exerted a greater influence on β than on α (see Table 6), owing to decrease in the stiffness of the lower part of the pylon. Furthermore, the variation in the 1st natural frequency was negligible.

4.2.2 Decrease in Sectional Area of Main Cable

The effect of decrease in the main cable area was opposite to that of the previous case, decrease in stiffness of for the lower part of the pylon. The parameter α decreased, since, for the same temperature variation, the generated unbalanced force was smaller than that resulting from the original cable area. Moreover, the rotation angle at the top of the pylon and the parameter β decreased (see Fig. 15), since the support stiffness k generated from the main cable had decreased.

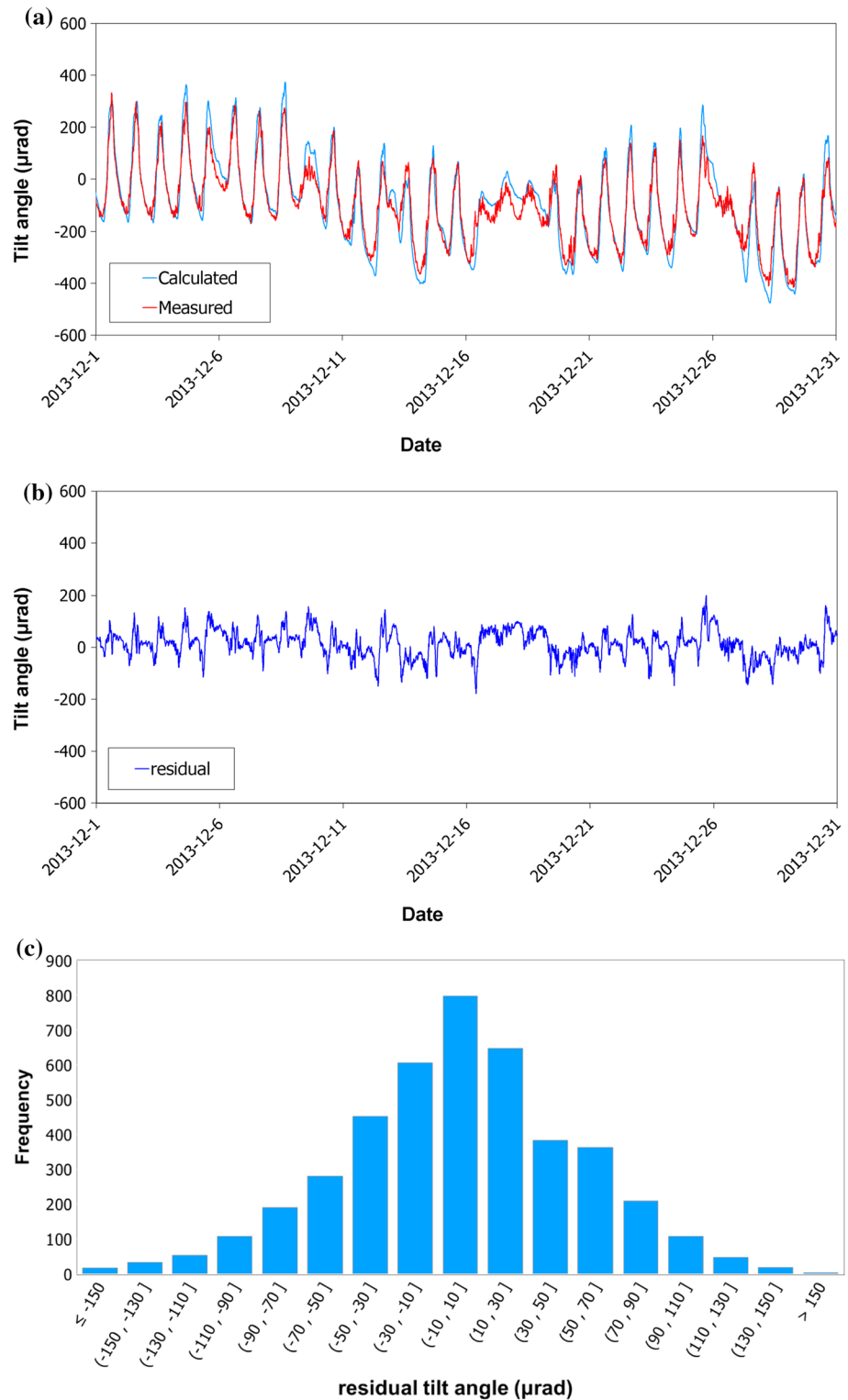
The results obtained for decrease in the main cable area are listed in Table 7. Similar ratios of change were obtained for both parameters (α and β) and the natural frequencies.

As mentioned previously, the influence of two major structural changes on the temperature parameters was examined via FE analyses. The results revealed that both parameters (i.e., α and β):

1. Increased due to decrease in the stiffness of the lower region of the pylon, and a greater influence on β was exhibited than on α .
2. Decreased due to decrease in the main cable area, and similar dependences were exhibited.

The temperature parameters may either increase or decrease, owing to decrease in the structural stiffness. Generally, a stiffness reduction results in increased deformation. However, decreased deformations occurred in these cases, due to the structural complexity of the suspension bridge.

Fig. 13 Analysis of residual error between measured and calculated tilting angle. **a** Measured and calculated tilting angle. **b** Residual error. **c** Histogram representing residual error



4.3 Influence of Structural Change on Tilting-Angle Response

Figure 16 shows the three sets of tilting-angle responses: the intact (DL_0), decrease in main cable area (DL_C2), and

decrease in stiffness of lower part of pylon (DL_P2), calculated using the temperature parameters listed in Tables 6 and 7. As shown in Fig. 16a, the three curves almost overlapped, and angles of the peaks measured between noon and 6 pm differ only slightly. A magnified view of these four peaks is

Table 3 Monthly residual errors

Month	SRSS error	Standard deviation (μrad)	Month	SRSS error	Standard deviation (μrad)
11	3470.7	52.8	5	3414.2	52.0
12	3442.0	52.4	6	3545.4	53.9
1	3869.6	58.9	7	3044.6	46.3
2	4150.3	63.2	8	2476.5	37.7
3	3743.1	57.0	9	3765.7	57.3
4	4464.2	67.9			

shown in Fig. 16b. We see from comparing Figs. 13 and 16 that the differences induced by changes in the temperature parameters were considerably smaller than the residuals between the measured and the calculated responses. Therefore, determination of structural changes via the analysis of field-measured data is difficult.

As mentioned previously, the major causes of the residuals between measured and calculated responses are traffic and wind loads. The wind load has no effect on the static response and, hence, the effect of the wind load can be eliminated via appropriate filtering. However, the traffic load results in both static and dynamic responses. Therefore, a method that nullifies the traffic-load effect is necessary for structural-change identification via analysis of field-measured data.

Taking into the effect of the traffic load was beyond the scope of this work, extraction of the two temperature parameters from the artificially generated response signals that do not incorporate traffic and wind load effects were thus attempted. Three sets of artificial signals were generated by adding random noise (assumed distribution: normal distribution, mean of distribution: zero, standard deviation: 20 μrad)

Table 4 Structural change 1 (decrease in stiffness of lower part of pylon)

Case ID	Wall thickness (mm)	Area (mm ²)	I _{yy} (mm ⁴)	I _{zz} (mm ⁴)
DL 0 (intact)	50	9.147E+5	2.461E+12	4.594E+12
DL P1	45	8.240E+5	2.222E+12	4.145E+12
DL P2	40	7.331E+5	1.982E+12	3.694E+12

Table 5 Structural change 2 (decrease in sectional area of main cable)

Case ID	Cable area (mm ²)	Area ratio (%)
DL 0 (intact)	226,700	100
DL C1	204,030	90
DL C2	181,360	80

to the calculated signals shown in Fig. 16a. Artificial signals for all three cases were generated over a 7-day period and, as Fig. 17a shows, visual distinction of these signals was impossible.

The temperature parameters were extracted from the artificial signals by solving an optimization problem (see Eq. (2)) using Excel Solver, which is based on a generalized reduced gradient (GRG) non-linear method. Both temperature parameters (α and β) and the constant C shown in Eq. (1) were determined by solving this problem.

$$\text{Minimize } \sum (Tilt_{measured} - Tilt_{calculated})^2 \tag{2}$$

where $Tilt_{measured}$ denotes the artificial signals (see Fig. 17). These signals were generated by summing the random noise and the responses calculated from the temperature parameters for the cases DL_P2 and DL_C2 (Tables 6 and

Fig. 14 Example of structural change. **a** Stiffness decrease for lower part of pylon. **b** Sectional area decrease for main cable

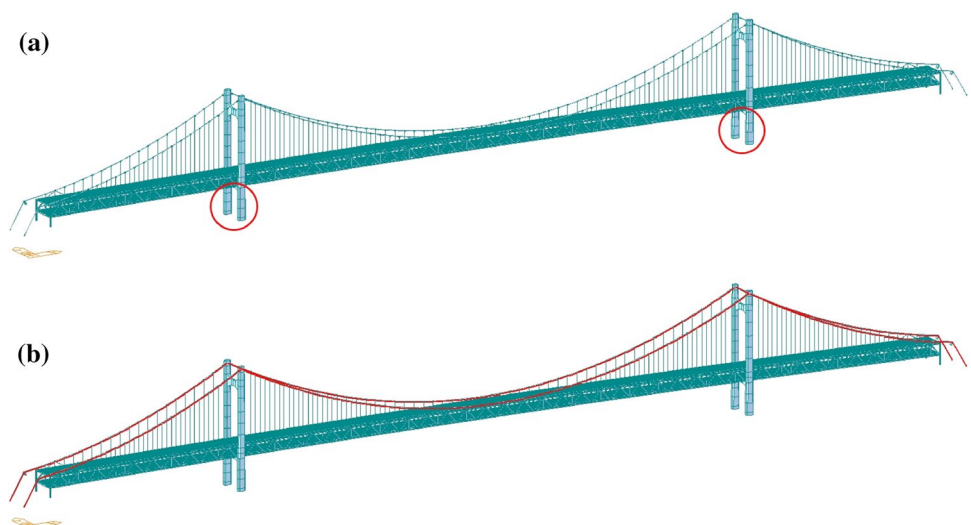
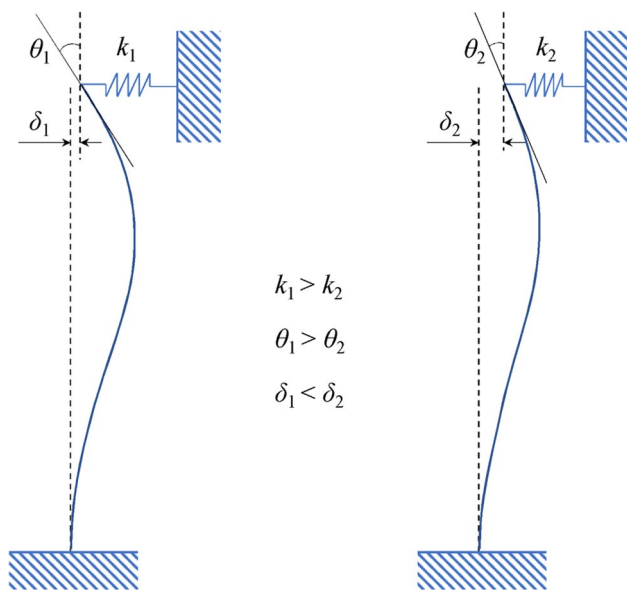


Table 6 Influence of structural change 1 (decrease in stiffness of lower part of pylon)

Case ID	Sensitivity to ambient temperature, α	Sensitivity to sectional difference, β	Natural frequency (1st vertical bending)
DL 0 (intact)	38.0 $\mu\text{rad}/^\circ\text{C}$	9.80 $\mu\text{rad}/^\circ\text{C}$	0.24185 Hz
DL P1	38.3 $\mu\text{rad}/^\circ\text{C}$ (+0.8%)	10.05 $\mu\text{rad}/^\circ\text{C}$ (+2.6%)	0.24177 Hz (−0.03%)
DL P2	38.7 $\mu\text{rad}/^\circ\text{C}$ (+1.8%)	10.33 $\mu\text{rad}/^\circ\text{C}$ (+5.4%)	0.24168 Hz (−0.07%)

**Fig. 15** Effect of decrease in main cable area on pylon tilting angle

7, respectively). Furthermore, $Tilt_{calculated}$ was determined from Eq. (1), which consists of three unknown variables α , β , and C .

The identified values for both parameters were compared with the exact values and, in each case (see Table 8), the deviation between these two sets of values (i.e., the error) was $< 1\%$. Consequently, precise identification from visually indistinguishable signals was possible.

5 Conclusion

The effect of structural changes (resulting from, for example, structural damage, structural deterioration, and long-term material behavior) on the temperature behavior of a long-span suspension bridge pylon was examined using field-measured data and FE analysis. The results revealed that the temperature behavior of the pylon could be described by two characteristic parameters, α and β , which reflect variations in the ambient temperature and variations in the sectional temperature difference, respectively. Both parameters varied with the two major structural changes considered in this study. Numerical analysis of the structural changes revealed that α and β both:

1. Increased due to decrease in the stiffness of the lower region of the pylon, and a greater influence on β was exhibited than on α .
2. Decreased due to decrease in the main cable area, and similar dependences were exhibited by them.

The results also confirmed that, by solving an optimization problem, these two parameters could be extracted with relatively high accuracy from the data corresponding to the air temperature, member temperature, and pylon tilting angle. However, further studies on eliminating other loading effects (such as effects due to wind and traffic loads) are necessary for structural-change identification via continuous observation of the temperature parameters.

Table 7 Influence of structural change 2 (decrease in sectional area of main cable)

Case ID	Sensitivity to ambient temperature, α	Sensitivity to sectional difference, β	Natural frequency (1st vertical bending)
DL 0 (intact)	38.0 $\mu\text{rad}/^\circ\text{C}$	9.80 $\mu\text{rad}/^\circ\text{C}$	0.24185 Hz
DL C1	37.4 $\mu\text{rad}/^\circ\text{C}$ (−1.6%)	9.68 $\mu\text{rad}/^\circ\text{C}$ (−1.2%)	0.23903 Hz (−1.16%)
DL C2	36.7 $\mu\text{rad}/^\circ\text{C}$ (−3.4%)	9.54 $\mu\text{rad}/^\circ\text{C}$ (−2.7%)	0.23541 Hz (−2.66%)

Fig. 16 Effect of structural change on pylon tilting-angle response. **a** Calculated tilting-angle curves. **b** Plot showing magnified peaks

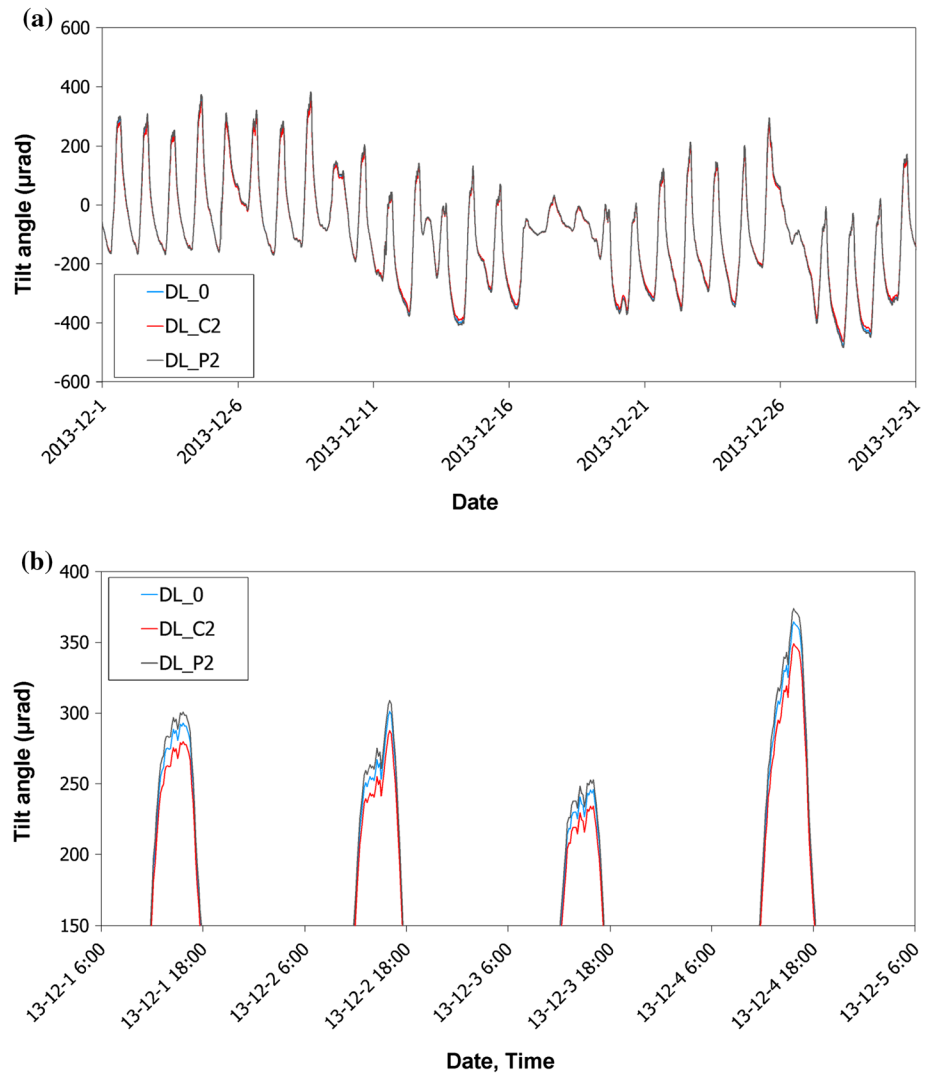


Fig. 17 Artificial-signal generation through addition of random noise. **a** Generated signal of tilting angle. **b** Distribution of added noise

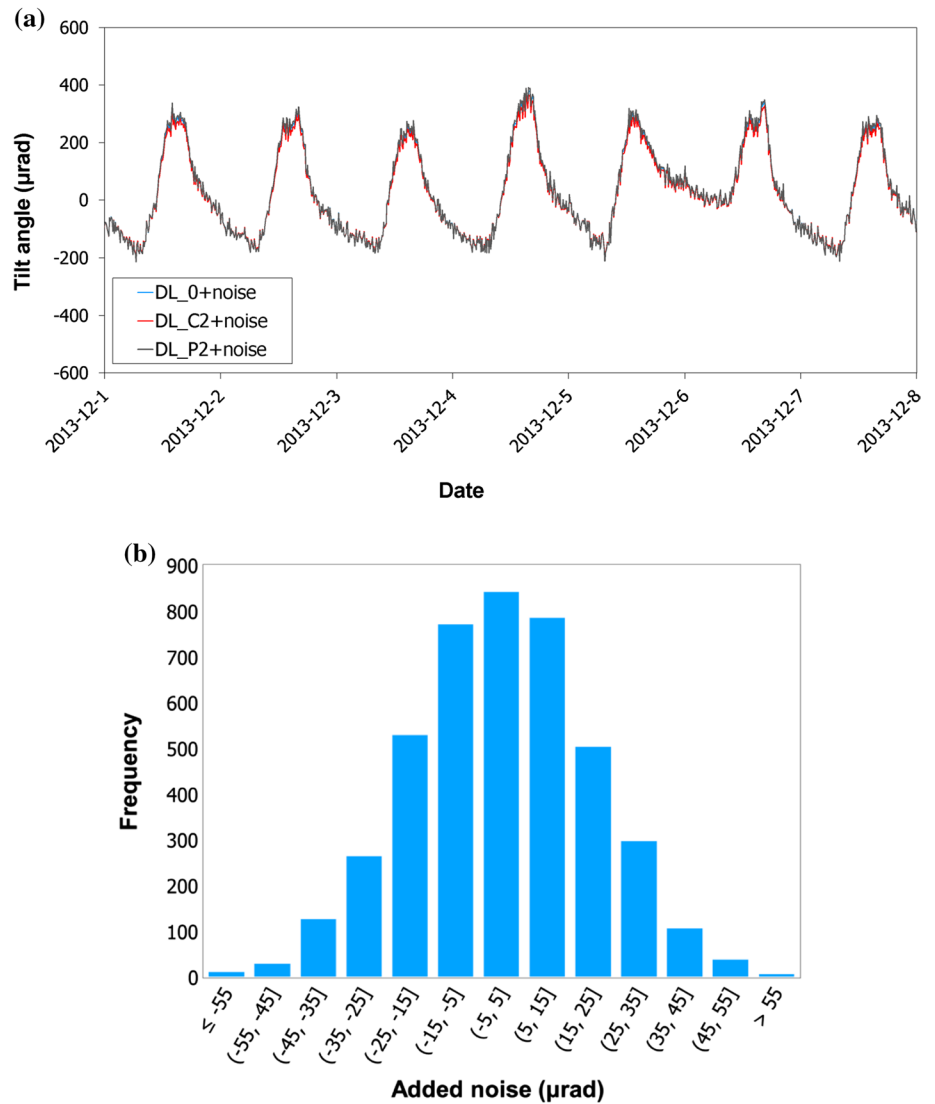


Table 8 Temperature parameters identified from artificial signals

Case ID	Sensitivity to ambient temperature, α			Sensitivity to sectional difference, β		
	Identified	Exact	Error (%)	Identified	Exact	Error (%)
DL 0	38.1	38.0	+0.26	9.72	9.80	-0.81
DL P2	38.8	38.7	+0.26	10.25	10.33	-0.77
DL C2	36.8	36.7	+0.27	9.46	9.54	-0.84

Acknowledgements The present research was conducted by the research fund of Dankook University in 2017. The authors are very grateful for the cooperation of the Busan Infrastructure Corporation (BISCO).

References

Cao, Y., Yim, J., Zhao, Yang, & Wang, M. L. (2010). Temperature effects on cable stayed bridge using health monitoring system: A

case study. *Structural Health Monitoring: An International Journal*, 10(5), 523–537.
 Chang, S. P., Kim, S., Lee, J., & Bae, I. (2008). Health monitoring system of a self-anchored suspension bridge (planning, design and installation/operation). *Structure and Infrastructure Engineering*, 4(3), 193–205.
 Chang, S. P., Yee, J., & Lee, J. (2009). Necessity of the bridge health monitoring system to mitigate natural and man-made disasters. *Structure and Infrastructure Engineering*, 5(3), 173–197.
 Fu, Y., & DeWolf, J. T. (2004). Effect of differential temperature on a curved post-tensioned concrete bridge. *Advances in Structural Engineering*, 7(5), 385–397.

- Kim, H. K., Kim, N. S., Jang, J. H., & Kim, Y. H. (2012). Analysis model verification of a suspension bridge exploiting configuration survey and field-measured data. *Journal of Bridge Engineering*, 17(5), 794–803.
- Kim, S., Kim, C. Y., & Lee, J. (2005). Monitoring results of a self-anchored suspension bridge. In F. Ansari (Ed.), *Sensing issues in civil structural health monitoring* (pp. 475–484). Dordrecht: Springer.
- Koh, H. M., Kim, S., & Choo, J. F. (2005). Recent development of bridge health monitoring system in Korea. In F. Ansari (Ed.), *Sensing issues in civil structural health monitoring* (pp. 33–42). Dordrecht: Springer.
- Koo, K. Y., Brounjohn, J. M. W., List, D. I., & Cole, R. (2013). Structural health monitoring of the Tamar suspension bridge. *Structural Control and Health Monitoring*, 20, 609–625.
- Liu, H., Chen, Z., & Zhou, T. (2013). Investigation on temperature distribution and thermal behavior of large span steel structures considering solar radiation. *Advanced Steel Construction*, 9(1), 41–58. <https://doi.org/10.18057/ijasc.2013.9.1.4>.
- Lynch, J. P., & Loh, K. J. (2006). A summary review of wireless sensors and sensor networks for structural health monitoring. *The Shock and Vibration Digest*, 38(2), 91–128.
- Magalhaes, F., Cunha, A., & Caetano, E. (2012). Vibration based structural health monitoring of an arch bridge: From automated OMA to damage detection. *Mechanical Systems and Signal Processing*, 28, 212–228.
- MIDAS Information Technology (MIDAS IT). (1996). *Midas civil-integrated solution system for bridge and civil structures*. MIDAS Information Technology, <http://www.MidasUser.com>
- Ou, J., & Li, H. (2010). Structural health monitoring in mainland China: Review and future trends. *Structural Health Monitoring*, 9(3), 213–219.
- Park, G., Kabeya, K., Cudney, H. H., & Inman, D. J. (1999). Impedance-based structural health monitoring for temperature varying application. *JSME International Journal, Series A*, 42(2), 249–258.
- Park, G., Sohn, H., Farrar, C. R., & Inman, D. J. (2003). Overview of piezoelectric impedance-based health monitoring and path forward. *The Shock and Vibration Digest*, 35(6), 451–463.
- Roberts-Wollman, C. L., Breen, J. E., & Cawrse, J. (2002). Measurements of thermal gradients and their effects on segmental concrete bridge. *Journal of Bridge Engineering (ASCE)*, 7(3), 166–174.
- Sohn, H., Dzwonczyk, M., Straser, E. G., Kiremidjian, A. S., Law, K. H., & Meng, T. (1999). An experimental study of temperature effect on modal parameters of the Alamosa Canyon Bridge. *Earthquake Engineering and Structural Dynamics*, 28, 879–897.
- Wong, K. Y. (2004). Instrumentation and health monitoring of cable-supported bridges. *Structural Control and Health Monitoring*, 11, 91–124.
- Xia, Y., Chen, B., Zhou, X. Q., & Xu, Y. L. (2013). Field monitoring and numerical analysis of Tsing Ma Suspension Bridge temperature behavior. *Structural Control and Health Monitoring*, 20, 560–575.
- Xu, Y. L., Chen, B., Ng, C. L., Wong, K. Y., & Chan, W. Y. (2010). Monitoring temperature effect on a long suspension bridge. *Structural Control and Health Monitoring*, 17, 632–653. <https://doi.org/10.1002/stc.340>.
- Yarnold, M. T., & Moon, F. L. (2015). Temperature-based structural health monitoring baseline for long-span bridges. *Engineering Structures*, 86, 157–167.
- Zhao, Z., Liu, H., & Chen, Z. (2017a). Field monitoring and numerical analysis of thermal behavior of large span steel structures under solar radiation. *Advanced Steel Construction*, 13(3), 190–205. <https://doi.org/10.18057/ijasc.2017.13.3.1>.
- Zhao, Z., Liu, H., & Chen, Z. (2017b). Thermal behavior of large-span reticulated domes covered by ETFE membrane roofs under solar radiation. *Thin-Walled Structures*, 115, 1–11.

Publisher's Note Springer Nature remains neutral with regard to jurisdictional claims in published maps and institutional affiliations.